University of Illinois at Urbana-Champaign

ACRC

Air Conditioning and Refrigeration Center  A National Science Foundation/University Cooperative Research Center

# Fin-Tube Junction Effects on Flow and Heat Transfer in Flat Tube Corrugated Multilouvered Heat Exchangers

D. K. Tafti and J. Cui

ACRC TR-190  January 2002

*For additional information:*

Air Conditioning and Refrigeration Center
University of Illinois
Mechanical & Industrial Engineering Dept.
1206 West Green Street
Urbana, IL 61801

(217) 333-3115

*Prepared as part of ACRC Project #114*
*Three-Dimensional Computational Modeling Of Augmented Louver Geometries for Air-side Heat Transfer Enhancement*
*D. K. Tafti, Principal Investigator*

*The Air Conditioning and Refrigeration Center was founded in 1988 with a grant from the estate of Richard W. Kritzer, the founder of Peerless of America Inc. A State of Illinois Technology Challenge Grant helped build the laboratory facilities. The ACRC receives continuing support from the Richard W. Kritzer Endowment and the National Science Foundation. The following organizations have also become sponsors of the Center.*

Alcan Aluminum Corporation
Amana Refrigeration, Inc.
Arçelik A. S.
Brazeway, Inc.
Carrier Corporation
Copeland Corporation
Dacor
Daikin Industries, Ltd.
Delphi Harrison Thermal Systems
General Motors Corporation
Hill PHOENIX
Honeywell, Inc.
Hydro Aluminum Adrian, Inc.
Ingersoll-Rand Company
Invensys Climate Controls
Kelon Electrical Holdings Co., Ltd.
Lennox International, Inc.
LG Electronics, Inc.
Modine Manufacturing Co.
Parker Hannifin Corporation
Peerless of America, Inc.
Samsung Electronics Co., Ltd.
Tecumseh Products Company
The Trane Company
Valeo, Inc.
Visteon Automotive Systems
Wolverine Tube, Inc.
York International, Inc.

*For additional information:*

*Air Conditioning & Refrigeration Center*
*Mechanical & Industrial Engineering Dept.*
*University of Illinois*
*1206 West Green Street*
*Urbana, IL 61801*

*217 333 3115*

## Abstract

Three-dimensional simulations of four louver-tube junction geometries are performed to investigate the effect on louver and tube friction and heat transfer characteristics. Three Reynolds numbers, 300, 600 and 1100, based on bulk velocity and louver pitch are calculated. Strong three-dimensionality exists in the flow structure in the region where the angled louver transitions to a flat landing adjoining the tube surface, whereas the flow on the angled louver far from the tube surface is essentially two-dimensional. Due to the small spatial extent of the transition region, its overall impact on louver heat transfer is limited, but the strong flow acceleration on the louver top surface augments the heat transfer coefficient on the tube surface by over 50%. In spite of the augmentation, the presence of the tube lowers the overall Nusselt number of the heat exchanger by over 30 %. Comparisons with correlations derived from experiments on full heat exchanger cores show that computational modeling of a small subsystem can be used reliably to extract performance data for the full heat exchanger.

# Nomenclature

| | |
|---|---|
| $D_H^*$ | Hydraulic diameter of equivalent duct |
| Fd* | Flow depth |
| Fp | non-dimensional fin pitch (Fp*/Lp*) |
| Lp* | dimensional louver pitch (characteristic length scale) |
| Nu | Nusselt number, $Nu = \frac{L_p^* q''^* / (T_s^* - T_{ref}^*)}{?}$ |
| Pr | Prandtl number |
| $q''^*$ | specified heat flux |
| Re | Reynolds number (ub*Lp*/ν) |
| $\mathrm{Re}_{L_p}$ | Reynolds number ( $V_c^* L_p^* / n$ ) |
| $\mathrm{Re}_{D_h}$ | Reynolds number ( $V_c^* D_H^* / n$ ) |
| $T_s^*$ | louver or tube surface temperature |
| $T_{ref}^*$ | reference temperature, integrated mixed mean. |
| t | non-dimensional time |
| ub* | bulk velocity |
| $V_c^*$ | Maximum mean flow velocity |

## Greek symbols

| | |
|---|---|
| γ | mean temperature gradient in the streamwise direction |
| κ | thermal conductivity |
| ν | kinematic viscosity |
| $q$ | fluctuating non-dimensional temperature about the mean. Also louver angle. |

## Superscripts

| | |
|---|---|
| * | dimensional quantities |

# 1. Introduction

Flat tube corrugated multilouvered fins are used in many compact heat exchanger applications to enhance the air-side heat transfer performance. Louvers reduce the average thermal boundary-layer thickness by interrupting its growth and by enhancing mixing through large-scale instabilities, hence increasing the average heat transfer coefficient. Previous experimental and numerical studies have established that the heat transfer in multilouvered fins is influenced by three factors: a) duct versus louver directed flow [1,2]; b) thermal wake interference [3]; c) flow instabilities and transport of coherent vorticity in the vicinity of the louver surface [4]. These three mechanisms have mostly been studied with a louver-centric view, i.e, heat transfer enhancement on a nominally two-dimensional louver, with the assumption that louvers contribute a significant portion to the overall heat transfer surface. For the most part this assumption is well justified. However, in exchangers with large fin pitches and small fin heights or tube pitch, the tube surface can contribute substantially to the total heat transfer. For example for a fin pitch of 1.5-2.0 times the louver pitch, and a tube pitch of 5 louver pitches, the tube surface area contributes between 30 to 40 percent of the total heat transfer area. This, coupled with the fact that the tube is the primary heat transfer surface with the largest potential for heat transfer, requires that attention be paid to the heat transfer from the tube surface.

Our specific geometry of interest is a flat tube multilouvered exchanger with corrugated rectangular channels. In order to gain some insight into what influences tube heat transfer, in this study we focus our attention on the region of the louver near the junction with the tube surface. In this region, along the height of the fin, the louver transitions from an angle $q$ to 0 degrees into a flat landing adjoining the tube surface as shown in Fig. 1(d)[1]. Cui and Tafti [5] numerically investigated the geometry in Fig. 1(d) at a Reynolds number of 1,100, based on louver pitch and bulk velocity. They found that although the flow on the angled portion of the louver was nominally two-dimensional with self-sustained flow oscillations characterized by spanwise vortices, the flow was strongly three-dimensional and unsteady in the transition region. A highly unsteady vortex jet formed at the leading edge, which was sucked under the louver. The jet was complemented by a region of strong flow acceleration in the vicinity of the top louver surface. Evidence was presented that the temporal evolution of the two was correlated, which had a significant impact on local heat transfer coefficients. In spite of the high heat transfer in this region, the overall effect on mean louver heat transfer was found to be small because of the small spatial extent of the transition region. However, It was found that the strong acceleration near the junction with the flat landing had a significant effect on tube heat transfer.

The objective of the present paper is to extend the previous three-dimensional unsteady simulations to study three Reynolds numbers, 1,100, 600 and 300. In addition to the Reynolds number effect, simulations are carried out on four variations of the transitional louver geometry to study the effect of geometry. The heat transfer and friction results are presented separately for the louver and tube, and combined to estimate the overall effect. Comparisons are also made with existing louver-and-tube correlations in the literature.

The paper is organized as follows: the numerical and computational method is presented in the next section, followed by the description of the louver geometries. In the section on results, the general flow features, louver and

[1] The corrugated fin curvature near the tube wall is neglected.

tube friction and heat transfer characteristics are discussed. Finally comparisons are made with experimental correlations. This is followed by concluding remarks.

## 2. Numerical formulation

We solve the non-dimensional, time-dependent, incompressible Navier-Stokes and energy equations in conservative form in generalized curvilinear coordinates. The governing equations for momentum and energy are discretized with a conservative finite volume formulation using a second-order central difference scheme on a non-staggered mesh. The Cartesian velocities, pressure, and temperature are calculated and stored at the cell center, whereas contravariant fluxes are stored and calculated at the cell faces. A projection method [6] is used for the time integration of the discretized continuity and momentum equations.

The louvered fin geometry is approximated by an infinite array of louvers in both streamwise and cross-stream directions, which results in a simpler system with periodic repetition of the basic unit. Periodic boundary conditions for velocity, modified pressure and temperature are applied in the streamwise and cross-stream directions since the flow is assumed to be both hydrodynamically and thermally fully developed without any entrance or exit effects. No-slip, no-penetration boundary conditions for velocity and constant heat flux conditions are enforced on the louver and tube surface.

More details of the numerical algorithm, treatment of the boundary conditions, verification and validation of the computer program and strategies for parallel computing can be found in Tafti et al. [7,8] and Cui and Tafti [5].

## 3. Description of four louver geometries

Four louver geometries are considered in this paper (see Fig. 1): (1) periodic louver; the louver is assumed periodic in the spanwise direction with no tube. This simulation isolates any intrinsic three-dimensional effects brought about by secondary three-dimensional instabilities [9]; (2) straight louver; the angled louver extends all the way to the tube; this serves as a baseline case to study the effect of louver geometry transition; (3) louver with transition without landing; the angled louver directly transitions to the tube surface; (4) louver with transition and flat landing, which has been studied in detail by Cui and Tafti [5] at Re=1100. Comparison of (3) and (4), highlights the role of the flat landing.

For all four geometries, the unit computational domain has a dimension of 1 (normalized by louver pitch $L_p^*$) in streamwise ($x$) direction, fin pitch 1 (in this particular case, fin pitch $F_p^*$ is same as $L_p^*$) in cross-stream ($y$) direction, and 2.5 in spanwise ($z$) direction along the fin height. Along the spanwise direction in geometry 4 (hereafter referred as *transition with landing*), the louver can be divided into three parts: angled louver (length, 1.75), transition part (length, 0.5), and flat landing (length, 0.25). A linear transition profile is prescribed between the angled louver and the flat landing with a small radii of curvature at the junction with the louver [10]. For geometry 3 (hereafter referred to as *transition without landing*), the angled louver part is extended to a length of 2.0, and the transition part is unchanged, but the flat landing between the transition and the tube surface is removed.

Geometry 2, referred to as a *straight louver*, has a spanwise extent of 2.5. Finally, geometry 1 is referred to as a *periodic louver* and has a spanwise extent of 2.5.

In all cases, the thickness of the angled louver is 0.1 times the louver pitch with 25° louver angle. For the last three geometries, symmetry boundary conditions are imposed at a distance of 2.5 from the tube surface along the fin height, assuming that the flow is sufficiently removed from the extrinsic three-dimensional effects of the tube wall region and is nominally two-dimensional. This also assumes implicitly that the fin height is 5.0 louver pitches. For the periodic louver, periodic boundary conditions are implemented in the spanwise direction since the flow is homogeneous along this direction.

The computational domain surrounding each louver is resolved by 98x98x128 computational cells in the *x*-, *y*- and *z*- directions, respectively for the transitioning geometries. For the periodic and straight louver, 96 computational cells are used in the *z*- direction along the fin height. A very fine, nearly orthogonal mesh, is used in the vicinity of the louver and tube surface, and in the transition region [5].

## 4. Results

In each of the calculations, a mean pressure gradient of unity is imposed in the streamwise direction to drive the flow. As the calculation proceeds, the flow rate, in response to the frictional and pressure drag losses in the calculation domain, adjusts to the mean pressure gradient and reaches a stationary (or steady state, in the case of low Reynolds number steady flow). Time signals of flow variables are recorded and a stationary flow is assumed when a near constant mean value or a quasi-periodic fluctuation in time is observed. Fig. 2 shows the temporal evolution of the spatially averaged Nusselt number for four louver geometries at a nominal Reynolds number of 1,100. It is clear that all flows have adjusted to the mean pressure gradient and reached a statistically stationary state. Similar plots at nominal bulk Reynolds number of 600 and 300 also show that the flow has reached a stationary or steady state.

To characterize the heat transfer, we define a local instantaneous Nusselt number over the louver surface based on the louver pitch as

$$Nu = \frac{L_p^* q''^* / (T_s^* - T_{ref}^*)}{?}$$

In terms of non-dimensional quantities the above can be re-written as

$$Nu = \frac{1}{?_s - ?_{ref}}$$

where $?_s$ [2] is the modified non-dimensional surface temperature and $?_{ref}$ is the reference modified non-dimensional bulk temperature, which is defined as :

[2] $T(x, y, z, t) = T_{in} + gx + q(x, y, z, t)$ , where $g$ is the mean temperature gradient.

$$?_{ref} = \frac{1}{V}\iiint ? \, dV$$

The surface-averaged Nusselt number is obtained by integration over the louver surface as:

$$Nu = \frac{\iint_O dS}{\iint_O (? - ?_{ref})dS}$$

where *W* denotes the louver surface. A similar procedure is used to calculate the *Nu* number on the tube surface. The Colburn *j* factor as a measure of heat transfer is calculated as:

$$j = \frac{Nu}{\mathrm{Re}\,\mathrm{Pr}^{0.4}}$$

The Fanning friction coefficient is calculated as:

$$f = \frac{\Delta p^*}{\frac{1}{2} r V_c^{*2}} \frac{D_h^*}{4F_d^*} = \frac{D_h}{2} \frac{1}{V_c^2}$$

where $D_h^*$ is the hydraulic diameter, $\Delta p^*$ is the prescribed pressure drop across the calculation domain (unity non-dimensional value in present calculations), and $V_c^*$ is the calculated maximum mean velocity.

### 4.1 General Flow Features

In the study of the louver with transition and flat landing [5], it is shown that flow on the angled louver portion is characterized by periodic spanwise vortex shedding at the Reynolds number of 1,100. The spanwise vortices are nominally two-dimensional in nature with weak three-dimensionality across the fin height. The time signal at a location above the top louver surface exhibits a nearly periodic pattern, and the frequency spectrum shows a clear peak at 1.8 (non-dimensionalized by bulk velocity and louver pitch), which corresponds to the frequency of the spanwise vortex shedding. At this Reynolds number of 1,100, all four louver geometries exhibit the same vortex shedding characteristic frequency. Although there is considerable geometry variation near the tube surface, its effects on the flow field on the louver away from the tube is minimal. Because of these similarities at the angled louver part, nearly identical flow and heat transfer behavior is expected for the four louver geometries. Any observable differences would come from the area near the tube surface.

At Reynolds number of 600, the flow unsteadiness becomes much weaker at the angled louver part. The time signals do not show a periodic pattern, and vortex shedding only occurs in an occasional manner, and there is no clear characteristic frequency. At Reynolds number of 300, the flow is completely steady and remains attached on the louver surface and there is no evidence of vortex shedding for all louver geometries. These results are in agreement with a previous two-dimensional investigation on the onset of instabilities for developing flow in a louver bank [4].

To facilitate our understanding of the unsteady nature of the flow and the associated vorticity dynamics, the ***Ñu*** [11] vortex identification technique is used. This frame-invariant method identifies vortical structures as regions

of large vorticity, where rotation dominates over strain to cause the rate-of-deformation tensor $\tilde{\nabla}\mathbf{u}$ (velocity gradient tensor) to have complex eigenvalues (one real and two conjugate complex eigenvalues). The complex eigenvalues imply that the local streamline pattern is closed or spiral, thus correctly eliminating near-wall shear layers. This methodology can also be separately applied in the *x*-, *y*-, or *z*- planes in order to identify streamwise, cross-flow, and spanwise vortices [9], respectively. The strength of the vortex is measured in terms of the imaginary part of the eigenvalue of the velocity gradient tensor and is denoted by $l_i$. The strength of its three subsets, streamwise, cross-flow, and spanwise vortices is measured in terms of the imaginary part of the eigenvalue of the velocity gradient on the *x*-, *y*-, and *z*- planes, respectively, and is denoted by $l_{i,x}$, $l_{i,y}$, and $l_{i,z}$, respectively.

Fig. 3(a-d) shows the volume-averaged vortical strength $l_{i,x,y,z}$ distribution along the fin height at an arbitrary instant at Reynolds number of 1,100[3]. Only the volumes with non-zero eigenvalues are included in the volume averaging. For the periodic case (Fig. 3-a), the lines for streamwise ($l_{i,x}$) and cross-flow ($l_{i,y}$) vorticity are identically zero throughout the louver height. The only contribution to the total vorticity is from the spanwise vorticity ($l_{i,z}$). Hence at Re=1,100, for the given louver geometry, the flow is strictly two-dimensional and intrinsic three-dimensional secondary instabilities have not developed[4]. For the straight louver, (Fig. 3-b), the spanwise vorticity dominates. However, there are small components of both streamwise ($l_{i,x}$) and cross-stream ($l_{i,y}$) vorticity present along the louver height. This implies that the three-dimensionality introduced by the presence of the tube wall permeates into the flow away from the wall and introduces weak three-dimensionality in a nominally two-dimensional flow. The spanwise vorticity ($l_{i,z}$) is damped considerably by the viscous presence of the wall which is felt up to one louver pitch away from it, implying very thick boundary layers on the tube wall. Approaching the tube surface, there is a noticeable but slight increase for both streamwise ($l_{i,x}$) and cross-flow ($l_{i,y}$) vorticity as the spanwise and total vorticity decrease.

For the louver with transition and flat landing (Fig. 3-d), on the angled louver, $l_i$ essentially maintains a constant value, with a dominant contribution from spanwise vorticity. However, in the transition region the flow is strongly three-dimensional. $l_i$ increases, with increasing contributions from streamwise and cross-stream vorticity, with a drop in contributions from spanwise vorticity. $l_i$ reaches a maximum in the center of the transition region and then decreases as the louver approaches the flat landing and the tube surface. The strong three-dimensionality at the transition region is related to the flow acceleration on the top surface and the vortex jet under the bottom louver surface at the transition region, which is described in detail in Cui and Tafti [5]. For transition without landing (Fig. 3-c), it is seen that the three-dimensionality at the transition region is weakened compared to transition with landing although the flow acceleration near the top louver surface and the vortex jet under the louver bottom surface at the transition region still exist. In the presence of the flat landing the acceleration on the top surface and the vortex jet feed off the streamwise flow along the flat landing. In the absence of the flat landing, when the louver transitions directly on to the tube surface, there is reduced access to fluid.

[3] To obtain the distribution, the volume averaging is performed in domains defined by decompositions used for parallel computation along the fin height.

[4] The nominally 2-D flow was perturbed by 3-D disturbances to seed any intrinsic three-dimensional secondary instabilities, but the perturbations were not self-sustaining.

### 4.2 Pressure and Friction Drag on Louver and Tube

Fig. 4(a-d) plots the fractional variation of mean form and friction drag per unit length along the fin height or spanwise direction at a nominal Re = 1,100[5]. For all four geometries, at the angled louver portion, the form drag dominates the friction drag and is almost unchanged throughout the angled louver. This is best exemplified by the two-dimensional flow over the periodic louver in Fig. 4(a), in which the form drag contributes 80 % to the overall pressure loss. For transition with landing (Fig. 4-d), and transition without landing (Fig. 4-c), the magnitude of pressure and friction drag is similar at the angled louver part. For the straight louver, although the form drag loss is four times the friction losses away from the tube surface, which is similar to other geometries, the contribution to total losses is dominated by the presence of the tube. Both frictional and form losses increase substantially in the vicinity of the tube surface because of viscous effects. As the flow approaches the tube, it slows down, and the flow angle reduces substantially, which leads to the increased contribution to form drag. For the transitioning geometries in Fig. 4(c) and (d), the trends are completely different. In the transition region, the form drag increases slightly and eventually vanishes at the flat landing. On the other hand, the friction drag increases sharply in the transition region and reaches its highest value near the flat landing due to the accelerating flow in that region before decreasing again on the flat landing. Similar, albeit weaker, distributions at the transition region is found for the transitioning geometry without the landing (Fig. 4-c).

Fig. 5(a-c) plots the mean drag force distribution as a function of the fin height for the transition with landing geometry at three Reynolds numbers: 1,100, 600, and 300. As the Reynolds number decreases, the contribution of pressure drag decreases while that of friction drag increases at the angled louver part. At a nominal Reynolds number of 300, the two drag forces are nearly equal. The distribution at the transition region and flat landing follow the same trend as the Reynolds number decreases. Overall the changes in Reynolds number do not change the salient features of the drag distribution throughout the louver. This is also true for the other three louver geometries.

Fig. 6 plots the fractional contribution of friction losses on the tube surface to the total losses. For all three geometries, the contribution of the tube to overall losses is less than 8 percent of the total for this geometry. The louvers with transition exhibit a higher contribution because of the increased shear stress on the tube surface as a result of the accelerating flow near it.

### 4.3 Time-averaged Heat Transfer Coefficient

Fig. 7(a-d) plots the time mean thermal field (modified temperature, $q$) on the top surface of the louver. Because the heat flux is fixed on the louver and tube surface, a high surface temperature implies low heat transfer. In all cases, at a nominal Re =1100, the shear layer at the leading edge of the louver separates and sheds vortices. Very near the leading edge, the heat transfer coefficients are high, but decrease in the recirculation zone which forms downstream of the leading edge. In the reattachment region, at half the louver length, the vorticity generated by the separated shear layer increases the heat transfer coefficient by increased mixing. For the periodic geometry, in the absence of any three-dimensionality, the surface temperature does not show any variations in the $z$-direction. For

[5] The form and friction drag are plotted as a fraction of the total losses. Since the mean pressure gradient is fixed at unity, the integrated area under the curves should add up to approximately 2.5, the pressure loss expressed as a force on the computational domain.

the straight louver, thick thermal boundary layers with high temperatures and low heat transfer coefficients exist in the vicinity of the tube. For transition with landing, in the transition region, the low temperature/high heat transfer region on the top surface near the flat landing is caused by unsteady flow acceleration in the vicinity of the louver surface. The flow acceleration still exists without the flat landing, but it results in weaker augmentation on the louver surface.

Temperature contours on the lower surface are shown in Fig. 8(a-d). For the periodic louver the heat transfer coefficient is a maximum at the leading edge and decreases thereafter till near the trailing edge where it increases again. A high temperature/low heat transfer region formed in the transition region in Fig. 8(c-d) result from the presence of the vortex jet. The jet is detached from the louver surface and a stagnant recirculating region is formed underneath the jet. Similar to the top surface, thick boundary layer near the tube surface exists for the straight louver on the bottom surface. Comparing temperature contours for both the transitional geometries on the top and bottom louver surfaces in the vicinity of the tube clearly shows the effect of flow acceleration on tube heat transfer. Temperature contours have lower values in the immediate vicinity of the tube on the top louver surface than on the bottom surface.

In Fig. 9(a-b), the average (time and spatial) Nusselt number on the louver, and tube surface is plotted separately. In Fig. 9(a), the periodic and straight louver exhibit the same Nusselt numbers. The presence of transition and the flat landing is detrimental to louver heat transfer. Since an angled louver always exhibits higher heat transfer than a flat plate, solely from the geometrical viewpoint, the presence of a transition region and a flat landing will result in lower heat transfer coefficients averaged across the fin height. The presence of the tube surface can further lower the average heat transfer coefficient on the louver. These effects can either be countered or reinforced further by other non-linear effects as observed (unsteady flow acceleration on louver top surface and vortex jet on bottom surface, separation) in the current study. The results indicate that the flow acceleration on the louver surface is not sufficient to counter the geometry effects of the louver straightening out. Hence, for best heat transfer on the louver, the transition region and flat landing should be kept as small as possible.

Contrary to this observation, the enhancement provided by the transition and flat landing on the tube surface is quite strong. The tube Nusselt number is lowest for the straight louver because there is nothing that can break the thick thermal boundary layer that forms on the tube surface. With the transitional louver, the unsteady flow acceleration on the top surface and to some extent the vortex jet under the louver, help to dilute the thermal boundary layer on the tube and increase heat transfer. Between the two transitional geometries, the presence of the small landing is quite favorable to heat transfer augmentation on the tube and a total augmentation between 75-100% is obtained when compared to the straight louver.

### 4.4 Overall Friction and Heat Transfer Coefficient for Flat Tube Louvered Heat Exchanger

In this section, the overall heat transfer and friction factors for an equivalent duct of aspect ratio 5, bounded by louvered fins and the tube surface are presented. These are compared to theoretical flow results for fully developed laminar flow in ducts. Fig. 10-a compares the calculated friction coefficient (*f*), and Fig. 10-b plots the equivalent Nusselt number ( $Nu_{D_h}$ ) versus $\mathrm{Re}_{D_h}$ .

The friction coefficient increases by a factor between 5 and 8 when compared to a fully-developed laminar flow in a duct of aspect ratio 5. On the other hand the Nusselt number is augmented by factors varying from 2.5 to 4. The tube surface results in approximately a 30% reduction in the overall Nusselt number. Hence, for small tube pitches and large fin pitches, tube surface heat transfer becomes critical to the performance of the heat exchanger. Between the three geometries, the louver with transition and flat landing exhibits the lowest friction coefficient, whereas the friction coefficient is highest in the absence of the flat landing. The former result is consistent with the fact that pressure losses are dominated by form drag, which is reduced substantially in the transition region and vanishes at the flat landing.

Finally we provide a comparison between the calculated results and previous experimental work. Both the calculated friction coefficient and Colburn *j*-factor are compared to relevant correlations available in the literature. This is provided to validate that computer models of a subsystem of the full heat-exchanger can provide results which compare favorably with experiments on full cores. The friction coefficient is compared to the correlation of Chang et al. [12], (referred to as CHLW) and the *j*-factor to the correlation by Chang and Wang [13] (referred to as CH), and also to that of Sunden and Svantesson [14] (referred to as SS). The SS correlation is specific to flat tube arrangements with corrugated louvers in rectangular channels, whereas both the *f*- and *j*- correlations are more general in nature and include a wide range of multilouvered geometries [12]. The following geometrical values are used in the correlations: fin pitch = 1(all lengths normalized by louver pitch), $q$ = 25 degrees, fin thickness = 0.1, fin height = tube pitch = 5, tube depth = 15, louver length = 4.5, major tube diameter = 1[6], and louver height as $0.5\sin q$.

Fig. 11(a-b) plot the *f*- and *j*- factor. Also plotted are upper and lower bounds of the experimental data from which the CHLW and CW correlations are derived. The calculated *f*- factor is higher than predicted by the correlation, but falls within the upper bounds of the experimental data. We also note that the current calculations are relevant to the type C geometry in Chang and Wang [13], which generally exhibits a higher friction coefficient than the other types of multilouvered geometries. Similarly, the calculated *j*-factors for the transitioning louver fall within the experimental bounds of the CW correlation but are lower than the SS correlation.

## 5. Conclusions

In this paper, we study the flow and heat transfer in four three-dimensional geometries (Fig. 1) of a flat tube corrugated multilouvered fins at three nominal Reynolds numbers: 1,100, 600, and 300. The four geometries vary in the configuration of the fin at the junction with the tube face. They range from completely neglecting the effect of the tube surface to including the realistic transition of the angled louver into a flat landing adjoining the tube face. The objective is to study the impact of this region on louver as well as tube heat transfer coefficients.

The results show that away from the tube surface, the flow is nominally two-dimensional with weak three-dimensionality. For louvers that flatten out into a flat landing, conditions are created for highly three-dimensional and unsteady flow phenomena. Flow in the transition region is characterized by unsteady acceleration on the louver

[6] Tube depth is used in the same context as flow depth. In our calculations, the flow depth is infinity. So a typical value of 15 is used. Similarly, the calculations do not simulate flow around the tube, so a value of 1.0 is assumed as the major tube diameter. In any case, for flat tubes, the contribution to pressure loss from the frontal area of the tube is negligible.

top surface and a vortex jet under the louver bottom surface. The flow acceleration has a large impact on louver heat transfer locally. However, its impact is minimal on the averaged heat transfer coefficient over the whole louver. It is concluded that for best louver heat transfer performance, the transition and flat landing should be kept as small as possible. On the other hand, the flow acceleration generated by the transitioning louver has a large impact on tube heat transfer and increases it by 50-75% over a straight louver, which does not transition to the tube surface.

Overall, it is found that the low heat transfer on the tube surface, decreases the overall heat transfer capacity of the heat exchanger by over 30 %. Hence, augmenting heat transfer on the tube surface is critical in small tube pitch, high fin pitch, multilouvered geometries. On the other hand, there is a minimal contribution (<8%) of tube frictional losses to total pressure losses.

The agreement of calculated results with correlations derived from full core experiments validates that realistic three-dimensional computational modeling of a small subsystem is a viable and effective tool in generating performance data for heat exchangers.

## 6. Acknowledgements

Dr. J. Cui was partially supported by the Air Conditioning and Refrigeration Center (ACRC), Department of Mechanical and Industrial Engineering, University of Illinois at Urbana-Champaign. Supercomputing time was granted by the NSF PACI program through the National Resource Allocation Committee (NRAC). The authors would like to acknowledge the contributions made by Dr. Weicheng Huang, University of Illinois Urbana Champaign, in mesh generation.

## 7. References

[1] C.J. Davenport, Heat Transfer and Flow Friction Characteristics of Louvered Heat Exchanger surfaces, *Heat Exchangers: Theory and Practice*, Taborek, J., Hewitt, G. F. and Afgan, N. (eds.), pp. 397-412, Hemisphere, Washington, D. C., 1983.

[2] R.L. Webb, and P. Trauger, Flow structure in the louvered fin heat exchanger geometry, *Experimental Thermal and Fluid Science*, 4, pp. 205-217, 1991.

[3] X. Zhang, and D.K. Tafti, Classification and effects of thermal wakes on heat transfer in multilouvered fins, *Int. J. of Heat Mass Transfer*, 44, pp. 2461-2473, 2001.

[4] D.K. Tafti, and X. Zhang, Geometry effects on flow transition in multilouvered fins — onset, propagation, and characteristic frequencies, *Int. J. of Heat Mass Transfer*, 44, pp. 4195-4210, 2001.

[5] J. Cui, and D.K. Tafti, Computations of flow and heat transfer in a three-dimensional multilouver fin geometry, Air Conditioning and Refrigeration Center TR-181, University of Illinois at Urbana-Champaign, Mechanical and Industrial Engineering Department, 2001. Also in review, *Int. J. Heat Mass Transfer*, submitted Sep. 2001.

[6] J. Kim, and P. Moin, Application of a fractional step method to incompressible Navier-Stokes, *J. Comput. Phys.*, 59, pp. 308-323, 1985.

[7] D.K. Tafti, L. Zhang, and G. Wang, Time-dependent calculation procedure for fully developed and developing flow and heat transfer in louvered fin geometries, *Numerical Heat Transfer, Part A*, 35, pp. 225-249, 1999.

[8] D.K. Tafti, X. Zhang, W. Huang, and G. Wang, Large-eddy simulations of flow and heat transfer in complex three-dimensional multilouvered fins, Invited paper, paper No. FEDSM2000-11325, CFD Applications in

Automotive Flows, 2000 ASME Fluids Engineering Division Summer Meeting, June 11-15, Boston, Massachusetts, 2000.

[9] L.W. Zhang, S. Balachandar, and D.K. Tafti, Effect of intrinsic three dimensionality on heat transfer and friction loss in a periodic array of parallel plates, *Numerical Heat Transfer, Part A*, 31, pp. 327-353, 1997.

[10] L.W. Zhang, personal communication, Modine Manufacturing Company, 2000.

[11] M.S. Chong, A.E. Perry, and B.J. Cantwell, A general classification of three-dimensional flow fields, *Physics of Fluids A* 2(5), pp. 765-777, 1990.

[12] Y.-J. Chang. K.-C Hsu, Y.-T. Lin, C.-C. Wang, A generalized friction correlation for louver fin geometry, *Int. J. Heat Mass Transfer*, Vol. 43, pp. 2237-2243, 2000.

[13] Y.-J. Chang and C.-C. Wang, A generalized heat transfer correlation for louvered fin geometry, *Int. J. Heat Mass Transfer*, Vol. 40, No. 3, pp. 533-544, 1997.

[14] B. Sunden, J. Svantesson, Correlations of *j*- and *f*-factors for multilouvered heat transfer surfaces, in: proceedings of Third UK National Heat Transfer Conference, pp. 805-811, 1992.

## List of Figures

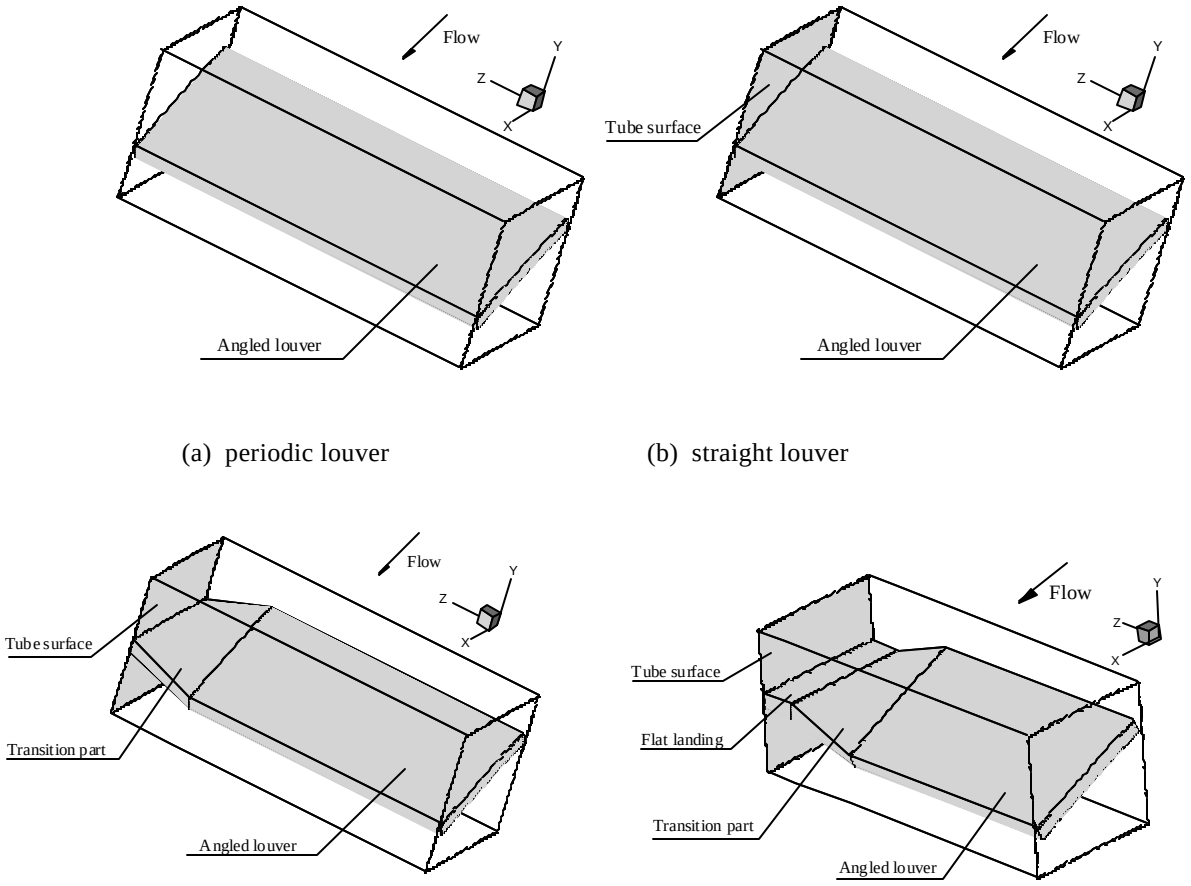


Figure 1. Computational domain for four louver geometries: (a) periodic louver; (b) straight louver; (c) transition without landing; (d) transition with landing. Shaded areas are the louver and tube surface.

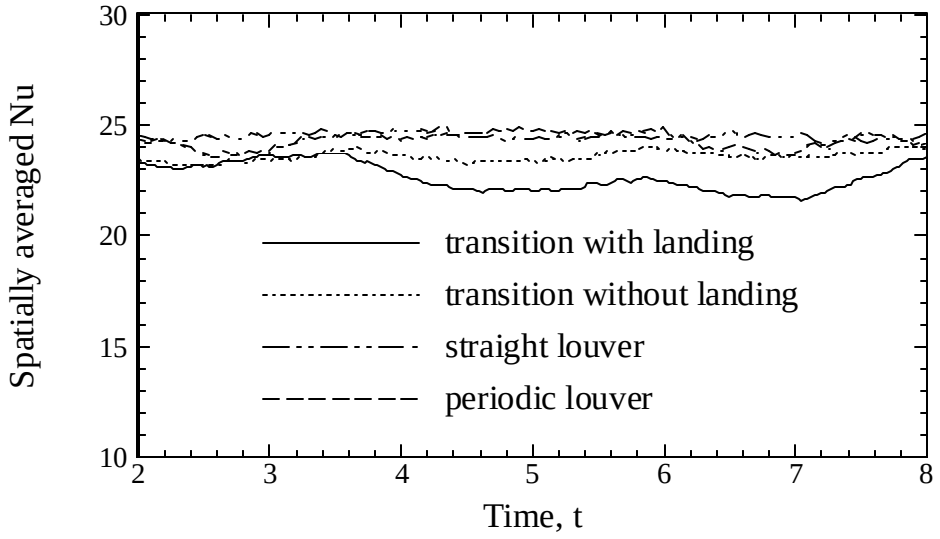


Figure 2. Temporal evolution of the spatially averaged Nusselt number for four louver geometries at Reynolds number of 1,100. All flows have adjusted to the mean pressure gradient and reached a statistically stationary state. Similar plots for louvers at Reynolds number of 600 and 300 also show that flow has reached a stationary state.

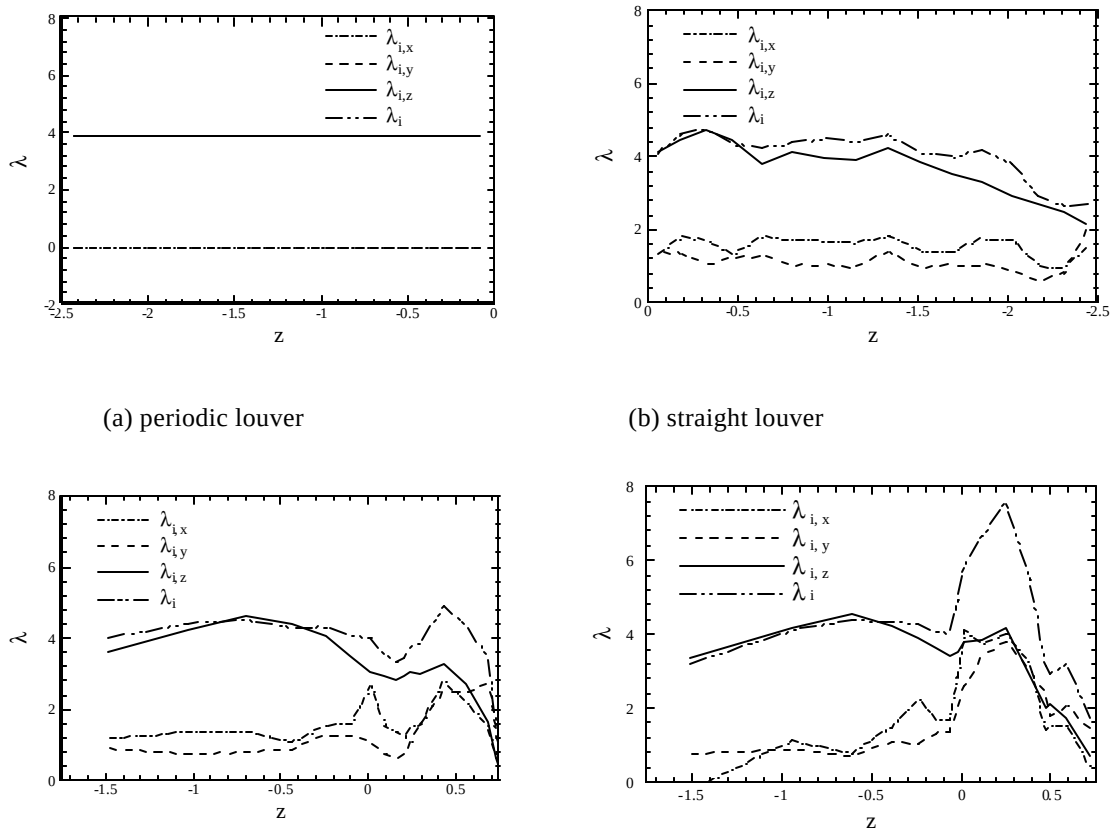


(a) periodic louver

(b) straight louver

(c) transition without landing

(d) transition with landing

Figure 3. Instantaneous volume-averaged vortical strength distribution along the fin height at Reynolds number of 1,100 at an arbitrary instant for (a) periodic louver; (b) straight louver; (c) transition without landing; (d) transition with landing.

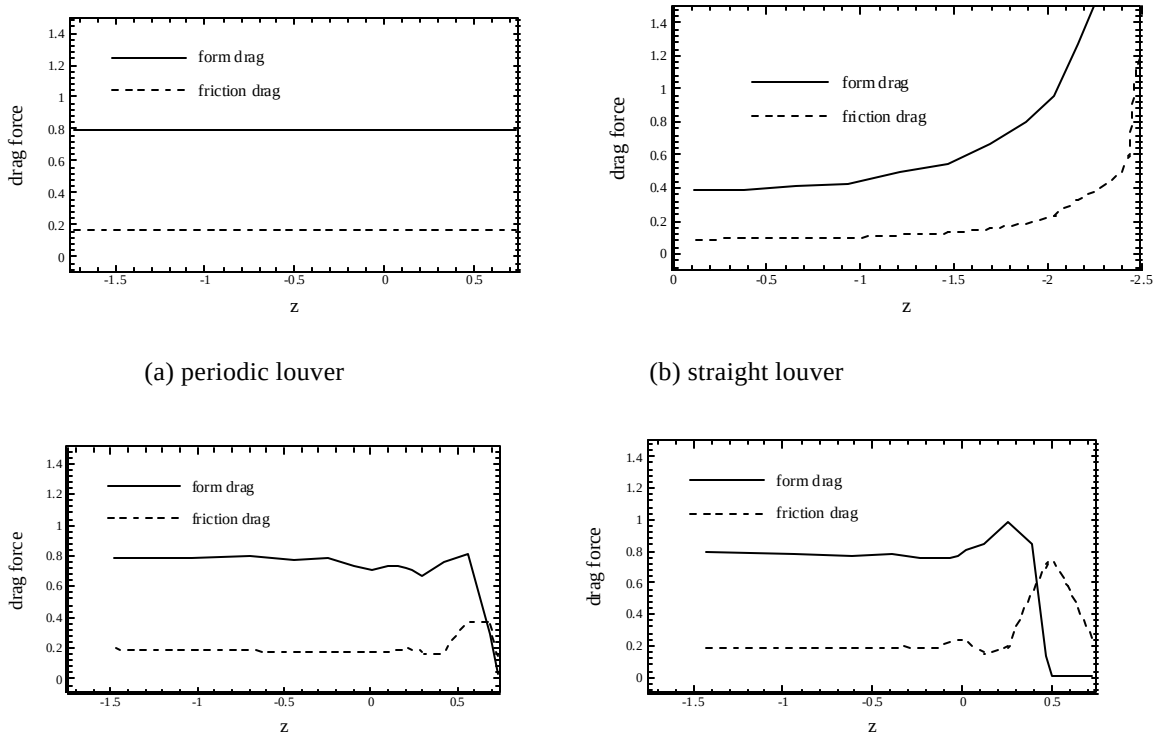


Figure 4. Mean drag force distribution along the fin height as a fraction of the total losses: (a) periodic louver; (b) straight louver; (c) transition without landing; (d) transition with landing at Reynolds number of 1,100.

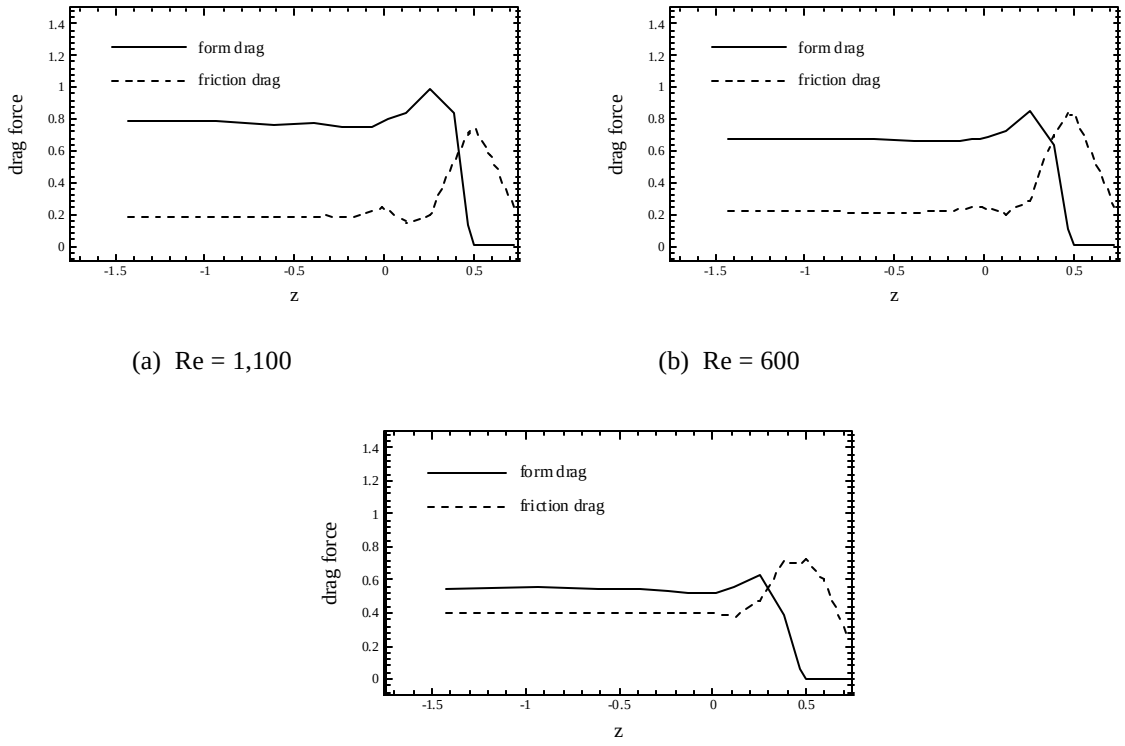


(a) Re = 1,100 (b) Re = 600

(c) Re = 300

Figure 5. Mean drag force distribution along the fin height as a fraction of the total losses for transition with landing at Reynolds number of (a) 1,100; (b) 600; (c) 300.

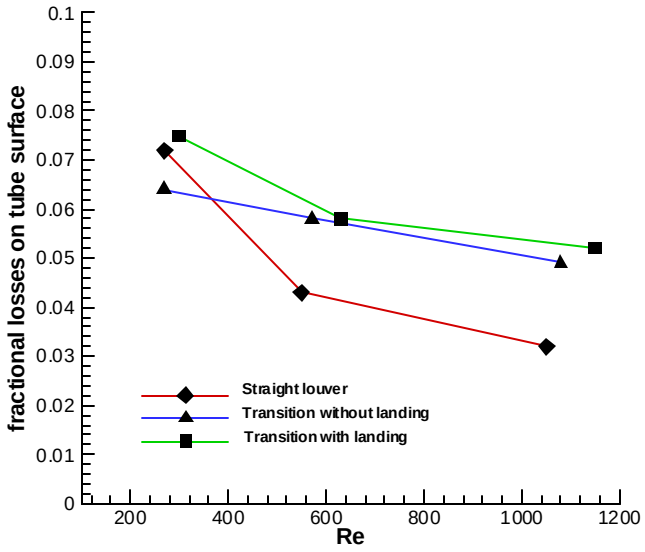


Figure 6. Fractional contribution of friction on tube surface to overall pressure loss.

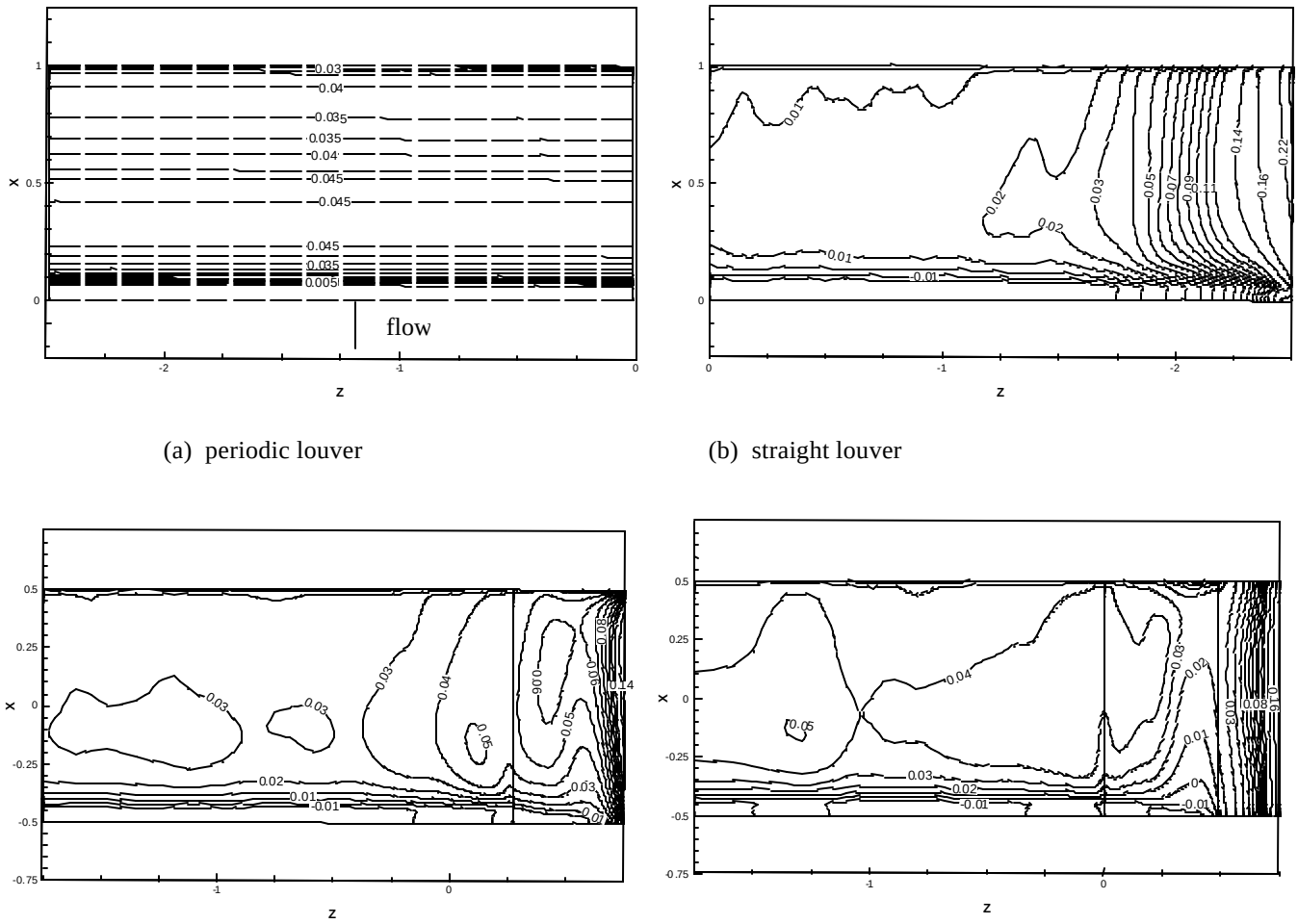


(a) periodic louver

(b) straight louver

(c) transition without landing

(d) transition with landing

Figure 7. Mean thermal field distribution on the louver top surface at Reynolds number of 1,100 for (a) periodic; (b) straight louver; (c) transition without landing; (d) transition with landing.

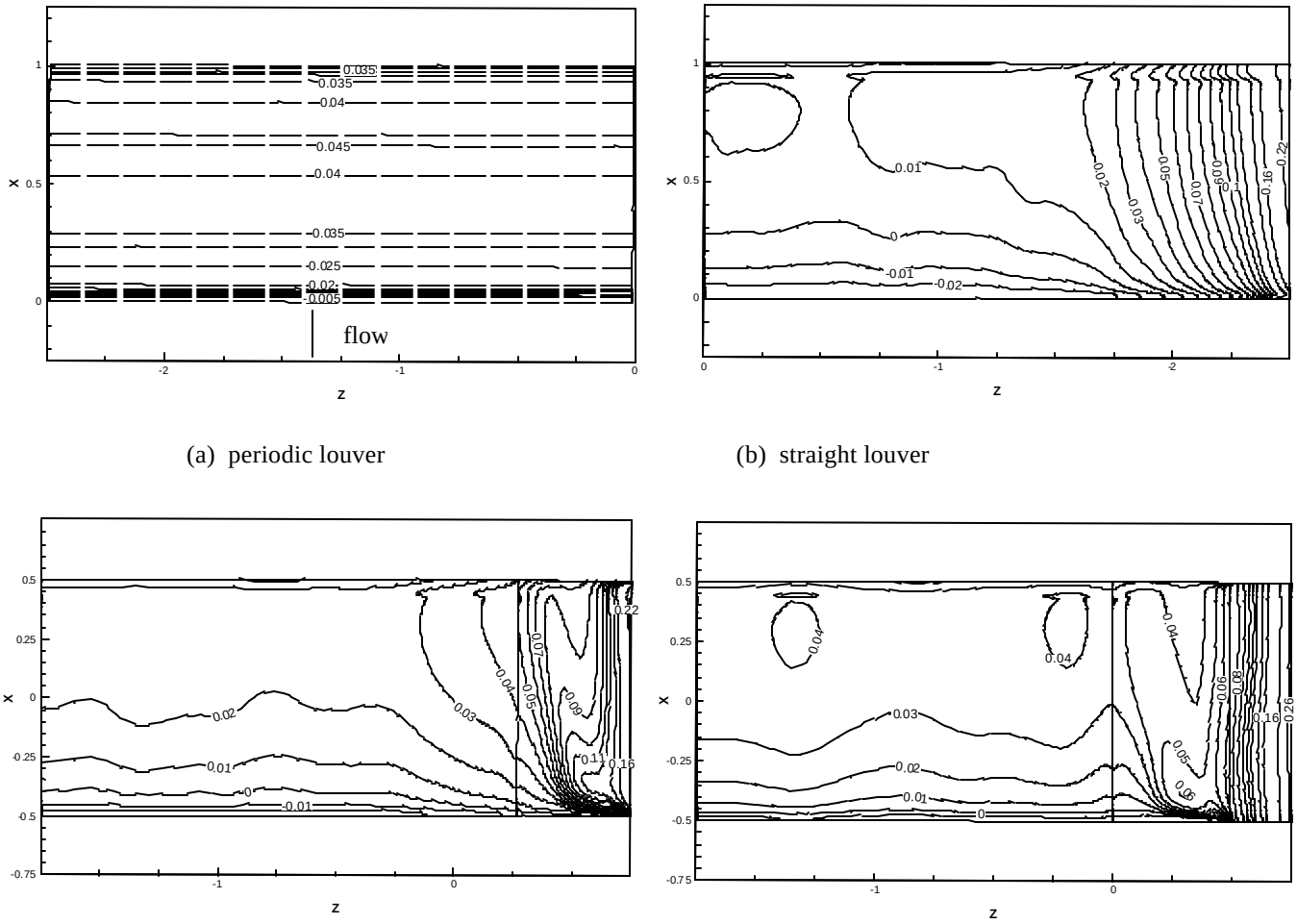


Figure 8. Mean thermal field distribution on the louver bottom surface at Reynolds number of 1,100 for (a) periodic; (b) straight louver; (c) transition without landing; (d) transition with landing.

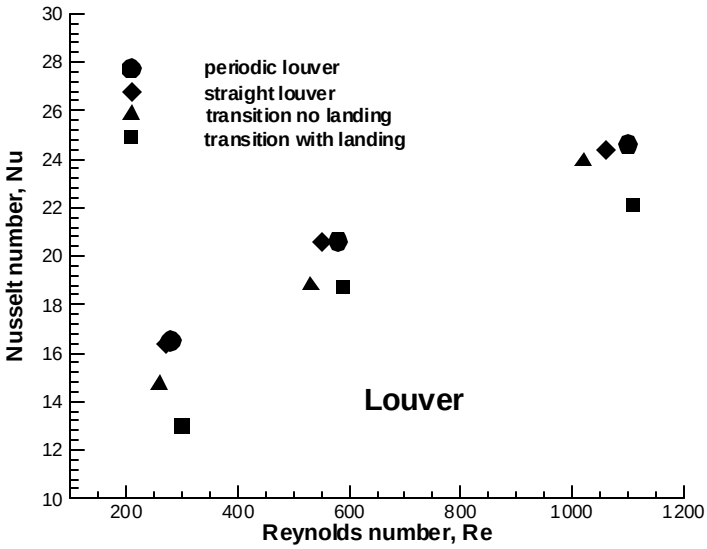


(a)

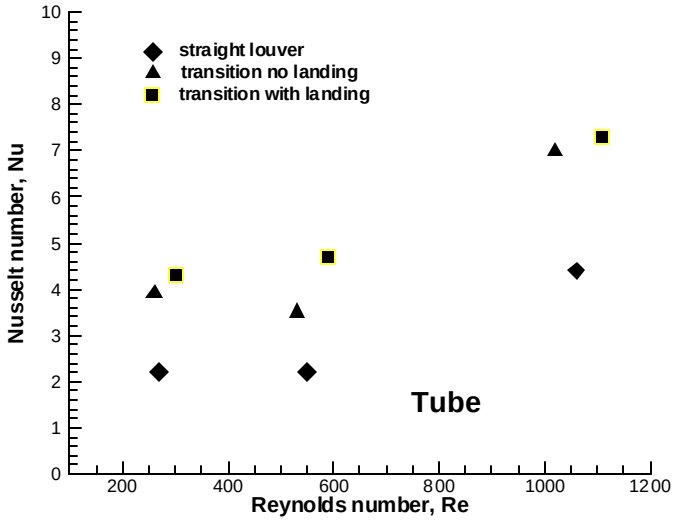


(b)

Figure 9. Average Nusselt number versus the Reynolds number. (a) On the louver surface; (b) On the tube surface.

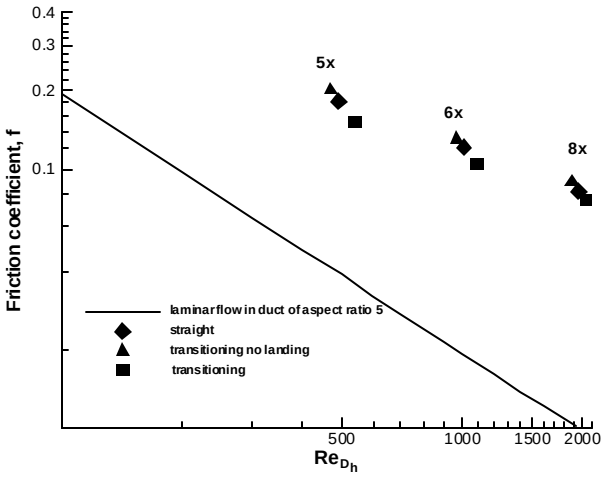


(a)

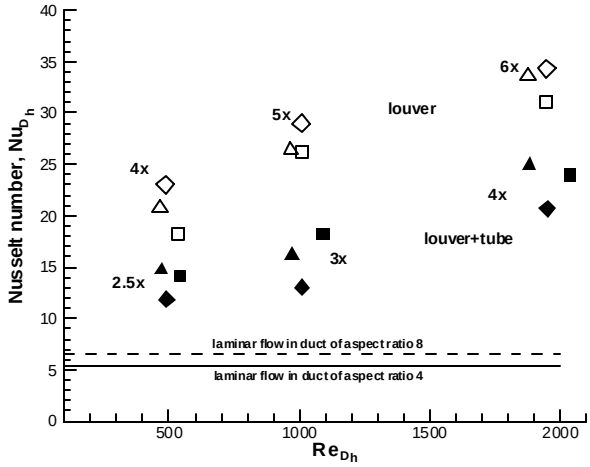


(b)

Figure 10. (a) Friction coefficient, $f$ for equivalent louvered duct; (b) Nusselt number for equivalent louvered duct. *Diamond*: straight louver; *delta*: transition no landing; *square*, transition with landing. *Empty symbols*: Nusselt number based on louver surface; *filled symbols*: Nusselt number based on louver and tube surface.

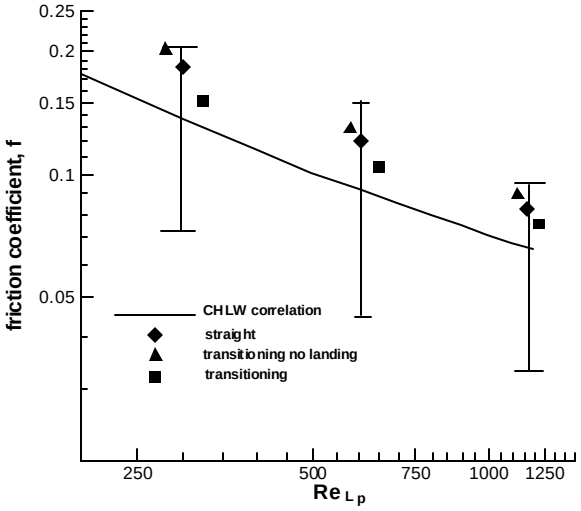


(a)

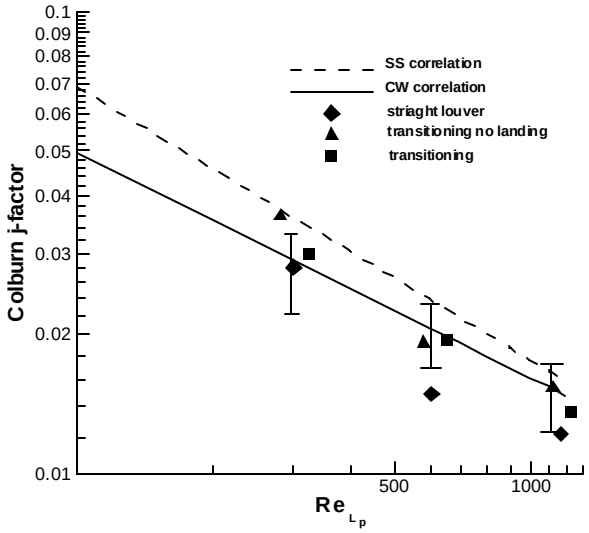


(b)

Figure 11. Comparison of calculated *f*- and *j*- factors with available correlations. Vertical lines establish limits of experimental data from which the CHLW and CH correlations were constructed.